Intraoral thermal processing in the gustatory cortex of awake mice.

Cecilia G. Bouaichi*, Camden Neese†, and Roberto Vincis§

§Florida State University, of Biological Science and Programs in Neuroscience, Molecular Biophysics and Cell and Molecular Biology
*Florida State University, Department of Biological Science, and Program in Neuroscience.
†Florida State University, Department of Biological Science.

February 6, 2023

Abstract

Oral temperature is a sensory cue relevant to food preference and nutrition. However, the cortical computation involved in processing thermosensory information in behaving animals remains largely elusive. In this study, we investigate how orally-sourced thermal inputs are processed in the gustatory cortex (GC), a cortical region typically studied for its role in processing another intraoral sensory cue - taste. Therefore, we used fiber photometry and electrophysiology to record neural responses from the GC of male and female mice presented with different innocuous temperatures (14 °, 25 ° and 36 °C) of deionized water. Our results demonstrate that GC neurons encode orally-sourced thermal information in the absence of taste, at both the single neuron and population level. Analysis of thermal-evoked responses showed broadly tuned neurons that responded to temperature in a mostly monotonic manner. Furthermore, spatial location plays a minor role with regard to thermosensory activity; with the exception of the most ventral GC, neurons reliably respond to and encode thermal information across the dorso-ventral and anterior-posterior cortical axes. Finally, decoding analysis revealed a small ensemble of GC neurons rapidly and accurately discriminate thermal information after the fluid is in contact with the mouth, providing additional evidence of the GC's involvement in processing thermosensory information important for ingestive behaviors. Altogether, our data reveal details of the cortical code for the mammalian intraoral thermosensory system in behaving mice and pave the way for future investigations on the GC functions and its operational principles with respect to thermogustation.

Introduction

The consumption of food and beverages is highly dependent on the initial sensation and the response it evokes (Dotson et al., 2012; Schier and Spector, 2019). This sensation arises within the mouth and involves the integration of intraoral gustatory, olfactory, and somatosensory cues in a single percept called flavor (Kemp and Beauchamp, 1994; Small, 2012). In the past decades, many electrophysiological studies in behaving rodents have investigated the physiological correlates of one of these intraoral sensory components – taste – which originates when chemical compounds stimulate specialized chemoreceptors within the oral cavity (Vincis and Fontanini, 2019; Spector and Travers, 2005). Using gustatory stimuli at a fixed temperature, these studies made clear that taste information is processed through neural computations that occur in interconnected brain areas that include the gustatory cortex (GC), the primary cortical area responsible for processing taste information (Katz et al., 2001; Jezzini et al., 2013; Stapleton et al., 2006; Liu and Fontanini, 2015; Samuelsen et al., 2013; Roussin et al., 2012; Bouaichi and Vincis, 2020; Levitan et al., 2019). In addition, these studies have indicated that GC neurons respond to compounds representing different taste qualities and their hedonic value with time-varying patterns of activity (Katz et al., 2001; Jezzini et al., 2013; Bouaichi and Vincis, 2020; Arieli et al., 2020; Neese et al., 2022) and play a role in driving taste-related decisions (Vincis et al., 2020; Mukherjee et al., 2019; Vincis and Fontanini, 2016).

However, a growing body of experimental work indicates that neurons in the GC are also capable of responding to non-gustatory components of intraoral stimuli (Bouaichi and Vincis, 2020; Stapleton et al., 2006; Rudenga et al., 2010; Samuelsen and Fontanini, 2017; De Araujo et al., 2003; Samuelsen and Vincis, 2021; Small et al., 2004; Maier, 2017), including temperature - a salient feature of the sensory properties of food and beverages. Different studies in humans and primates (Verhagen et al., 2004; Cerf-Ducastel et al., 2001; Guest et al., 2007), as well as pioneering works in anesthetized rats (Yamamoto et al., 1981; Kosar et al., 1986), have indicated that changes in intraoral temperature seem to modulate activity in GC neurons. While these data implicate the GC as a potential key cortical region for the integration of taste and thermal orosensory inputs, they stop short of supplying a fine-grained analysis of its neural responses, and many questions remain. Here, using fiber photometry and extracellular recording (tetrodes and silicon-based probes), we aim to provide a complete neurophysiological assessment of how thermal orosensory inputs shape GC activity in alert mice in the absence of taste. Specifically this study is designed to assess 1) whether and how neurons in the GC of actively licking mice are modulated by changes in the temperature of a chemically inert drinking solution and 2) the spatial organization of intraoral thermal-related information across the GC. To this end, GC neural activity was recorded while mice actively experienced a 4 µl water droplet at three different non-nociceptive temperatures (14 °, 25 °, and 36 °C).

Our data provide novel insights into how thermal information originating from the mouth is integrated in the neurons of a central structure associated with taste. Our findings demonstrate that more than half of the neurons recorded throughout the GC encode water information in a temperature-dependent and mostly monotonic manner. In addition, the analysis of our data suggests that thermal stimulation inside the mouth evokes responses that are organized in a coarse topographic manner along the dorso-ventral axes of the GC and that intraoral thermal signals are reliably encoded over time, with high accuracy. Overall, our results are consistent with the GC being an integral component of the cortical network involved in processing intraoral thermosensory signals and point to its potential role as a central brain region involved in the integration and communication of behaviorally relevant thermo- and chemosensory information.

Materials and Methods

Data acquisition

The experiments in this study were performed on 21 wild type C57BL/6J adult mice (10-20 weeks old; 11 males and 10 females) that were purchased from The Jackson Laboratory (Bar Harbor, ME). Upon arrival to the animal facility, animals were housed on a 12h/12h light-dark cycle and had ad-libitum access to food and water. Experiments and training were performed during the light portion of the cycle. All experiments were reviewed and approved by the Florida State University Institutional Animal Care and Use Committee (IACUC) under protocol "PROTO202100006".

Surgery

All animals were anesthetized with an intraperitoneal injection of a cocktail of ketamine (25 mg/kg) and dexmedetomidine (0.25 mg/kg). The depth of anesthesia was monitored regularly via visual inspection of breathing rate, whisker reflexes, and tail reflex. Anesthesia was supplemented by $\frac{1}{4}$ the original dose of ketamine as needed throughout the surgery. A heating pad (DC temperature control system, FHC, Bowdoin, ME) was used to maintain body temperature at 35 °C. At the start of surgery, mice were also dosed with dexamethasone (0.4 mg/kg, intramuscular) and bupivacaine HCl (2%, subcutaneous). In addition, lactate solutions were administered every 0.5 h during surgery at volumes of 0.5 ml. Once a surgical plane of anesthesia was achieved, the animal's head was shaved, cleaned and disinfected (with iodine solution and 70% alcohol) before being fixed on a stereotaxic holder.

Fiber photometry: Mice (n = 5; 2 males and 3 females) were infused unilaterally with adeno-associated virus (AAV) expressing the genetically encoded calcium indicator GCaMP7s (AAV9-syn-jGCaMP7s-WPRE, Addgene, Watertown, MA). A small craniotomy was drilled above the GC (AP: +1.2; ML:+3.5 from bregma). A pulled glass pipette front-loaded with the viral construct was lowered into the GC (-2.0 mm

Mouse ID	Probe	Date "Exp. session"	Mouse ID	Probe	Date "Exp. session"
CB279	Tetrodes	121421	CB278	Tetrodes	121521
CB279	Tetrodes	121621	CB278	Tetrodes	121721
CB279	Tetrodes	122021	CB278	Tetrodes	121921
CB295	Tetrodes	033022	CB293	Tetrodes	040222
CB295	Tetrodes	040222	CB293	Tetrodes	040422
CB295	Tetrodes	040422	CB293	Tetrodes	040622
CB300	Tetrodes	061522	CB301	Tetrodes	062422
CB300	Tetrodes	061722	CB301	Tetrodes	062722
CB300	Tetrodes	062022	CB301	Tetrodes	070322
CB311	Tetrodes	081022	CB312	Tetrodes	081022
CB311	Tetrodes	081222	CB312	Tetrodes	081222
CB311	Tetrodes	081522	CB312	Tetrodes	081522
CB280	Tetrodes	121521	CB313	Tetrodes	081222
CB280	Tetrodes	121721	CB313	Tetrodes	081522
CB313	Tetrodes	081722	CB289	CN-H5	040422
CB321	CN-H5	113022	CB316	CN-H5	040422
CB305	CN-H5	062722	CB303	CN-P1	061522
CB317	CN-P1	110822	CB303	CN-P1	061722
CB317	CN-P1	111022	CB303	CN-P1	062022

Table 1: List of all the experimental sessions.

from brain surface). 300-500 nl of virus was injected at 1 nl/s with a microinjection syringe pump (Nanoject III, Drummond Scientific Company, Broomall, PA). Following injection, we waited an additional five minutes before slowly pulling the pipette out. Optical fibers (200 µm diameter, 0.37 numerical aperture, Neurophotometrics, San Diego, CA) were implanted unilaterally 0.1 mm dorsal to the infusion site to allow subsequent imaging of calcium transients in the GC neurons. The optical fiber and a head screw (for the purpose of head restraint) were cemented to the skull with dental acrylic. Animals were allowed to recover for a minimum of 7 days before the water restriction regimen and training began.

Electrophysiology: To record extracellular activity, mice (N = 16; 9 males and 7 females) were implanted with a custom-made movable bundle of 8 tetrodes [the same used and described in (Vincis et al., 2020; Bouaichi and Vincis, 2020; Neese et al., 2022); N = 10 mice] or with one of two types of chronic and movable silicon probes mounted on a nanodrive shuttle (Cambridge Neurotech). One (H5, Cambridge Neurotech; N = 4 mice) had a single shank with 64 electrodes (organized in two adjacent rows spaced 22.5 µm apart) evenly spaced at 25-µm intervals. The other (P1, Cambridge Neurotech; N = 2 mice) had four shanks separated by 250 µm, where each shank had 16 electrodes (organized in two adjacent rows spaced 22.5 µm apart) evenly spaced with 25-µm intervals. Craniotomies were opened above the left GC for implanting tetrodes and probes and above the visual cortex for implanting ground wires (A-M system, Cat. No. 781000). Tetrode bundles, the H5 probes, and the anterior shank of the P1 probes were implanted at AP: +1.2 mm and ML: +3.5 mm (relative to bregma) and were slowly lowered above GC (1.5 mm below the cortical surface). Movable bundles and P1 probes were further lowered 300 µm before the first day of the "control session" recording. H5 probes were further lowered 1200 µm before the first day of the "control session" recording. Tetrodes or probes and a head screw (for the purpose of head restraint) were cemented to the skull with dental acrylic. Before implantation, tetrode wires and the tip of the silicon probes were coated with a lipophilic fluorescent dye (DiI; Sigma-Aldrich), allowing us to visualize their exact locations at the end of each experiment. Animals were allowed to recover for a minimum of 7 days before the water restriction regimen and training began.

Data collection

Fiber photometry: Fiber photometry was used to image intraoral thermal-evoked bulk calcium activity in GC neurons (Fig. 1). We simultaneously imaged GCaMP7s and control fluorescence in the GC using a commercial fiber photometry system (Neurophotometrics Ltd., San Diego, CA). Two light-emitting LEDs (470 nm: GCaMP fluorescence; 415 nm: autofluorescence, motion artifact) were reflected off dichroic mirrors and coupled via a patch cord (fiber core diameter, 200 µm; Doric Lenses) to the implanted optical fiber. Fluorescence traces were collected at 20 Hz, interleaved between the 415 and 470 excitation channels, using a custom Bonsai pipeline (Lopes et al., 2015). The time stamps of task events (licking and stimulus delivery) were collected simultaneously through a MATLAB (MathWorks, Natick, MA) based behavioral acquisition system (BPOD, Sanworks) synchronized with the Bonsai software.

Electrophysiology: Voltage signals from the tetrodes and probes were acquired, digitized, and band-pass filtered with the Plexon OmniPlex system (Plexon, Dallas, TX) (sampling rate: 40 kHz). The time stamps of task events (licking and stimulus delivery) were collected simultaneously through a MATLAB (MathWorks, Natick, MA) based behavioral acquisition system (BPOD, Sanworks) synchronized with the OmniPlex system.

Experimental Design and Statistical Analysis

Behavioral apparatus and training.

One week before training began, mice were mildly water restricted (1.5 ml/day) and maintained at or above 85% of their pre-surgical weight. One week after the start of the water restriction regimen, mice were habituated to be head restrained for short (5 minute) daily sessions that gradually progressed (over days) toward longer sessions. During restraint, the body of the mouse was covered with a semicircular opaque plastic shelter to constrain the animal's body movements without stressful constriction (Fig. 1A). The fluid delivery system, licking detection, and behavioral paradigm were described in detail in previous studies from our group (Bouaichi and Vincis, 2020; Neese et al., 2022). Following the habituation to restraint, mice were trained with a fixed ratio schedule in which the mice learned to lick a dry spout six times to trigger the delivery of the small water drop. Fluid was delivered via gravity by computer-controlled 12 V solenoid valves (Lee Company) calibrated daily to deliver 4 µl from a licking spout (Bouaichi and Vincis, 2020; Neese et al., 2022). A peltier block device (ALA Scientific, NY) located close to the tip of the licking spout was used to heat or cool the water to a specific temperature. The licking spout was made of short polyamide tubing (ID 0.03, MicroLumen) exiting the peltier block. The peltier can be heated or cooled to various temperatures between 0 °C and 50 °C by altering the polarity and the magnitude of DC current provided by a central amplifier. This in turn led to heating or cooling of an aluminum block, through which the licking tube passed. To calibrate the temperature of the drinking solution, a thermocouple probe was placed at the exit of the licking spout, and the equipment was considered calibrated when the thermocouple reliably read the desired value of fluid temperature. Therefore, the setting of the temperature (with the associated polarity and value of the DC current) on the central amplifier was based upon the temperature of the fluid exiting the licking spout and not the one within the peltier block. During the habituation and recording sessions (see below for more details), mice received a single 4 µl droplet of nanopure water (Barnstead/Thermolyne Nanopure lab water system) at one of three temperatures (14 °, 25 °, or 36 °C). These temperatures were chosen for three main reasons: 1) they are outside the range of overt noxious thermal stimuli (Suzuki et al., 2003; Allchorne et al., 2005), allowing the animal to be engaged in the task and actively lick for a substantial number of trials (allowing proper statistical analysis of neural data); 2) they provide compatibility to behavioral studies in rodents that investigated the role of water temperature on intake and preference (Torregrossa et al., 2012; Kay et al., 2020); 3) they represent a broad range of rewarding qualities in water-deprived rodents - with colder stimuli being perceived as more rewarding (Torregrossa et al., 2012). To separate neural activity evoked by the intraoral stimuli from neural correlates of sensory and motor aspects of licking, we 1) trained the mice to receive each intraoral stimulus on a fixed ratio schedule, 2) trained the mice for up to two weeks before recording, allowing for familiarization with the different stimuli, and 3) did not analyze any imaging or ephys recording session if the licking pattern evoked by each intraoral stimulus was not similar across at least a 1.5-s temporal window (Fig. 1C), as defined by a Kruskal Wallis test. As a result, the

neural response evoked by the tastants were compared with the one elicited by licking the dry spout before stimulus delivery. This also served to make sure that neural activity evoked by the distinct intraoral stimuli would not be impacted by differences in stimulus-evoked licking variables. Water-temperature pairings were presented in a block design, with 10 trials for each block and at least six blocks per session. For the electrophysiology experiments, to successfully locate the GC, we relied not only on stereotaxic coordinates and post-hoc evaluation of probes track (see Fig. 2B) but also on physiological mapping. To this end, we used the "control session" to record the neural activity evoked by different taste qualities and water presented at room temperature (∼22 °C). After this recording session, single neuron spiking activity was analyzed. In the case in which taste-responsive neurons were detected, we proceeded with recording GC neurons while mice performed exclusively the "experimental session" for up to three daily sessions. Otherwise the animals were removed from the study (n = 2 mice). At the end of each "experimental session", tetrodes and P1 probes were further lowered in order to sample new GC neuron ensembles (up to three recording sessions per mouse; see Table 1). For recording sessions with tetrodes, bundles were lowered ∼100 µm after recording each "experimental session" (Table 1). For recording sessions with P1 probes, they were lowered 200 µm after recording each "experimental session" (Table 1). For recording sessions with H5 probes, we analyzed only the neural recording obtained during one "experimental session" (Table 1).

Fiber photometry data and statistical analysis

Fluorescence data were pre-processed using a custom-written pipeline in MATLAB (MathWorks, Natick, MA). Data from the 415-nm isosbestic control channel were used to correct for motion artifacts and photobleaching. First, we fitted the 415-nm traces with biexponential decay. Second, we linearly scaled the former fit to the 470-nm data with a linear regression model. Finally, the change in fluorescence ($\Delta F/F$) at each time point was calculated by subtracting the scaled fit from the 470 signal and normalizing to scaled fit data [(470-scaled fit)/(scaled fit)]. Using a custom MATLAB workflow, $\Delta F/F$ traces were then aligned to water delivery for each trial.

Electrophysiology data and statistical analysis

Kilosort 2 (tetrode data) and Kilosort 3 (probe data) (Pachitariu et al., 2016) were used for automated spike sorting on a workstation with an NVIDIA GPU, CUDA, and MATLAB installed. Following spike sorting, Phy software was used for manual curation. Finally, quality metrics and waveform properties were calculated using code based upon SpikeInterface (Buccino et al., 2020). Only units with an overall firing rate > 0.3 Hz, signal to noise ratio > 3.0 and an ISI violation rate < 0.2 were used for the subsequent analyses. All following analyses were performed on custom Python scripts.

Water-responsiveness: Water-responsiveness was assessed in all isolated neurons (n = 431). This analysis was performed on data averaged across temperatures and therefore serves only to estimate whether and how many GC neurons were responsive to water, not whether that response depends upon the temperature of the stimulus.

Single-unit spike timestamps were aligned to the stimulus delivery and peri-stimulus time histograms (PSTHs) were constructed (bin size = 100 ms). ROC analysis was then used to compare the firing rates between baseline and evoked activity in a 1.5-s window before and after fluid delivery. Specifically, the area under the ROC curve (auROC) was used to calculate the responsiveness index. Responsiveness index ranged from 0 to 1, where 0 meant higher firing rate before the stimulus (baseline), 1 meant higher firing rate after the stimulus (evoked), and 0.5 meant similar firing rate between baseline and evoked activity.

To assess the significance of the responsiveness index, we used a permutation test where baseline/evoked trials were shuffled without replacement. Data were shuffled 1000 times and the pseudo responsiveness index was calculated for each iteration of the shuffling. The p-value was computed by comparing the actual responsiveness index with the pseudo index. We used a criteria $p < 0.01$ to determine significance. Neurons with significant responsiveness index were defined as water-responsive (see Fig. 3). Response latency onset and peak for water-responsive neurons were assessed as follows.

Latency onset was defined as the time in which the smoothed PSTH trace reached half of the max (for active responses where baseline firing rate < evoked firing rate) or the min (for suppressed responses where

baseline firing rate > evoked firing rate) firing rate. Latency peak was defined as the time in which the smoothed PSTH trace reached the peak (for active responses) or the valley (for suppressed responses) firing rate.

Temperature-selective neurons: To determine the degree of temperature specificity of GC water responses, we subjected each of the water-responsive neurons to a support vector machine (SVM) classifier, used and described in detail in a previous study (Neese et al., 2022). Briefly, the spike train dataset (0-1.5 s after water delivery) was transformed into a collection of vectors, each corresponding to one experimental trial. Each trial in the dataset was classified hierarchically according to neuron ID and temperature of water (labels: 14 °, 25 °, or 36 °C) for the trial. Thus, several vectors are associated with a single neuron, depending on how many trials were run with different temperatures. Then, for each single neuron, the classification analysis consisted of separating the ensemble of vectors into a training set consisting of 67% of the spike trains, and a testing set consisting of the remaining 33% of the spike trains. The training set was used to fit parameters for the SVM model (linear SVM kernel was used throughout our analysis); the SVM searched for hyperplanes that best separated the various classes (i.e., points corresponding to trials for different water temperatures) within the dataset. The trained model was then used to classify the testing dataset, resulting in a classification score measured as the percentage of correctly classified points. This procedure was repeated 20 times for each neuron, each time using a different partition of vectors into training and testing sets, and the classification scores were averaged over these trials to obtain an overall classification score for the neuron. To assess the significance of the overall classification score, we used a permutation test where the labels of the trials were shuffled without replacement. Spike trains were shuffled 1000 times and the pseudo classification score index was calculated for each iteration of the shuffling. A neuron was deemed temperature-selective if its overall classification score was > 99%ile of the pseudo classification scores (p <0.01).

Population decoding classifier: To understand how well the GC encoded information regarding intraoral temperature, we used a population decoding approach. To this end we first constructed a pseudopopulation of GC neurons using temperature-selective neurons recorded across different sessions (n = 137). We then generated a firing rate matrix (trials × time bin) where the spike timestamps of each neuron (2 s before and 2 s after stimulus) were realigned to water delivery, binned into 50-ms time bins. To assess the amount of temperature-related information, we used the SVM classifier described above. Spike activity data contained in our matrix were divided into training set consisting of 67% of the spike trains and a testing set consisting of the remaining 33% of the spike trains. This process was repeated 20 times (each time using different training and testing splits) to compute the decoding accuracy, defined as the fraction of trials in which the classifier made correct temperature predictions using a 25 ms sliding window. To assess the significance of the population decoding over time, we used a permutation test where the labels of the trials were shuffled without replacement. Spike trains were shuffled 10 times and the pseudo classification score over time was calculated for each iteration of the shuffling.

Histology

At the end of the experiment, mice were terminally anesthetized and perfused transcardially with 30 ml of PBS followed by 30 ml of 4% paraformaldehyde (PFA). The brains were extracted and post-fixed with PFA for 24 h, after which coronal brain slices (100 µm thick) containing the GC were sectioned with a vibratome (VT1000 S; Leica). To visualize the GCaMP7s expression and the optic fiber placement as well as the tracks of the tetrode bundles and probes, brain slices were counterstained with Hoechst 33342 (1:5,000 dilution, H3570; ThermoFisher, Waltham, MA) by standard techniques and mounted on glass slides. GC sections were viewed and imaged on a fluorescence microscope.

Results

Population representation of intraoral thermal inputs with calcium imaging

To start investigating if and how GC neurons encode intraoral thermal information in the absence of taste, we recorded population neural activity in freely licking mice activity using calcium imaging (Fig. 1, n = 5

mice: 3 males and 2 females).

After habituation to head restraint, water-deprived mice were engaged in a fixed-ratio (FR) task in which they had to lick 6 times to a dry spout to obtain a 4-µl drop of water at one of three non nociceptive temperatures (14 °, 25 °, and 36 °C) (Fig. 1).

Mice were trained and familiarized with the different temperatures until the licking pattern evoked by each of the individual intraoral stimuli was similar across a 1.5-s temporal epoch following delivery (Fig. 1C; see method for more details). Figure panels 1D-E show the trial-by-trial heat-map representation of calcium transients evoked by water at the three different temperatures (Fig. 1D) and the peri-event plots of the Ca^{2+} transients averaged over trials (Fig. 1E). Visual inspection of the graphs indicated that water delivery reliably evoked Ca^{2+} transients across trials (Fig. 1D) and that GC neurons were differently activated by intraoral temperature as reflected in the temporal profile of the stimulus-evoked calcium responses. In addition, a quantitative evaluation of the stimulus-evoked calcium transients in five mice further indicated that GC population neural activity appeared to be dependent on the temperature of the fluid stimulus (Fig. 1F; Welch Two Sample t-test; t = 2.8569, df = 4.7616, p-value = 0.03759). These results show that stimulus-evoked activity in the GC appear to be modulated by the temperature of the fluid solution in the absence of taste.

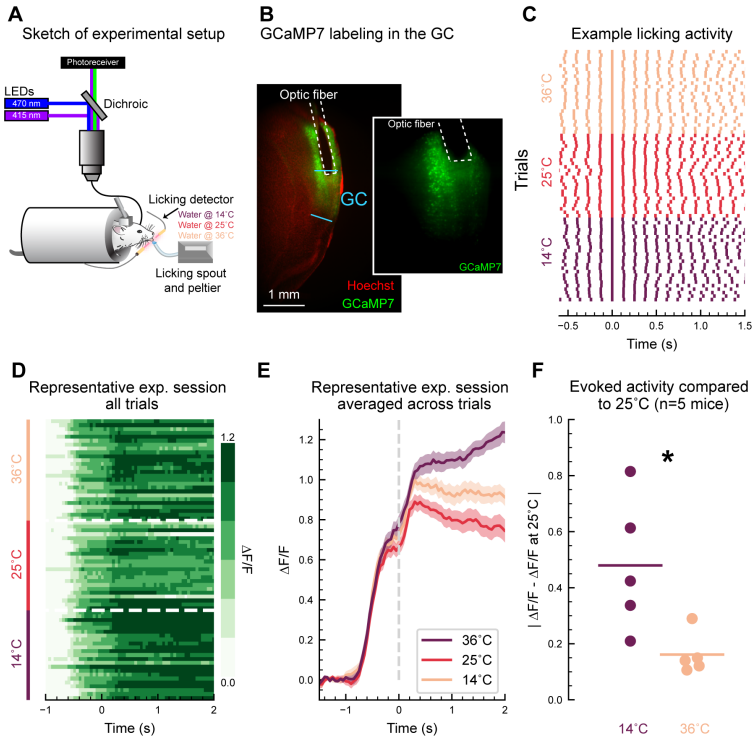

Figure 1: Fiber photometry results. A: Sketch showing the recording setup and a head-restrained mouse licking a spout to obtain water stimuli at three different non-nociceptive temperatures (14 °, 25 °, and 36 °C). B: Low and high (inset) magnification of the viral expression of AAV-GCaMP7s and placement of the fiber-optic cannula in the GC. C: Raster plot of licking activity. Each line represents an individual lick; trials pertaining to water at different temperature are grouped together and color-coded. Water delivery occurs at time 0 s. D: Representative session showing the trial-by-trial heat-map representation of calcium transients evoked by water at the three different temperatures. Trials pertaining to water at different temperature are grouped together and separated by horizontal white dashed lines. E: Peri-event plots of the calcium transients averaged over the trials of the same session shown in *D*. The gray vertical dashed line at time 0 s highlights water delivery. F: Quantification of changes in calcium activity evoked by 14 °and 36 °C across mice (n = 5; 3 males and 2 females). ΔF/F is normalized with the activity evoked by water at 25 °C. (Welch Two Sample t-test; t = 2.8569, df = 4.7616, p-value = 0.03759)

Single neuron analysis of GC thermal responses

We used fiber photometry to start examining the effect of intraoral temperature on the activity of GC. However, fiber photometry data acquisition is limited to population-level activity with no cellular resolution to record individual neurons. To investigate how single GC neurons encode intraoral thermal information in freely licking mice, we recorded ensembles of single units via movable bundles of tetrodes (Vincis et al., 2020; Bouaichi and Vincis, 2020; Neese et al., 2022) or movable silicon probes (Cambridge Neurotech) mounted on a nanodrive shuttle (Cambridge Neurotech) implanted unilaterally in the GC (Fig. 2). As mentioned above, after habituation to head restraint, water-deprived mice were engaged in the FR7 task in which they had to lick 6 times to a dry spout to obtain a 4-µl drop of one intraoral fluid stimulus. On alternating days for up to 10 days, mice were trained to receive either five gustatory stimuli (sucrose, 200 mM; NaCl, 50 mM; citric acid, 10 mM; quinine, 0.5 mM; water) at room temperature ("control session"; Fig. 2A) or only water at three different temperatures (14 °, 25 °, or 36 °C; "experimental session"; Fig. 2A). During this training, tetrode bundles or silicon probes were slowly lowered to their final position as described in the methods section. At the end of the training, the recording session began. First, we recorded neural activity evoked by different taste qualities and water presented at room temperature ("control session"; Fig 2D). After this recording session, single neuron spiking activity was analyzed; if taste-responsive neurons were

detected, in the next recording sessions, we exclusively recorded activity evoked by water at the different temperatures ("experimental session"; Fig. 2E; 3 recording sessions for all mice except the ones implanted with the H5 probe; at the end of each experimental session, tetrodes and probes were lowered to record new ensembles of neurons [see Materials and Methods section for more details]; Table 1). It is important to highlight we are not claiming we tracked the same taste-responsive neurons across multiple recording days. However, this approach provided additional evidence to support that recordings aimed at neuron responses to orally-sourced thermal stimuli were obtained from the GC. A total of 431 single neurons were recorded from 16 mice with an average yield of 11.42 ± 6.49 neurons per session. To begin evaluating the neural dynamics evoked by intraoral thermal stimuli in active licking mice, we analyzed the spiking profile of single GC neurons. Figure 2E shows the raster plots and PSTHs of two representative GC neurons.

Visual inspection of the graphs indicated that each of these neurons was modulated by different temperatures of water (Fig. 2E). As a first step, we wanted to understand how many GC neurons were modulated by the presence of a solution in the mouth. This analysis was performed on data averaged across temperatures and therefore serves only to estimate whether and how many GC neurons were responsive to water—not whether that response depended upon the temperature of the stimulus. To this end, we compared the firing rate during baseline to the spiking activity evoked by water. Au-ROC analysis revealed that a substantial number of the recorded GC neurons [59.9% (258/431)] responded to water stimuli and were classified as "water-responsive" (Fig. 3A-B). We observed that 37.6% (162/431) of water-responsive neurons displayed an excitatory response (water-evoked firing rate > baseline firing rate), whereas 22.3% (96/431) displayed an inhibitory response (water-evoked firing rate < baseline firing rate)(Fig. 3A-B). Figure 3C shows the population averages (population PSTHs) of the excitatory and inhibitory responses. When comparing the sign of water-responsive neurons, we observed significant differences between the number of water-responsive neurons that show an excitatory vs. inhibitory response. This last observation holds true when comparing the overall fraction of responsive neurons (Fig. 3A; Chi-squared test for given probabilities: X-squared = 16.884, df = 1, p-value = 3.974e-05) and also when comparing the proportion of GC cell-stimulus pairs that showed activation or suppression of the stimulus-evoked firing rate (Fig. 3D; Two Sample t-test: t = 3.7713, df = 74, p-value = 0.0003246). Analysis of the distribution of the latency of the responses indicated that the majority of water-responsive

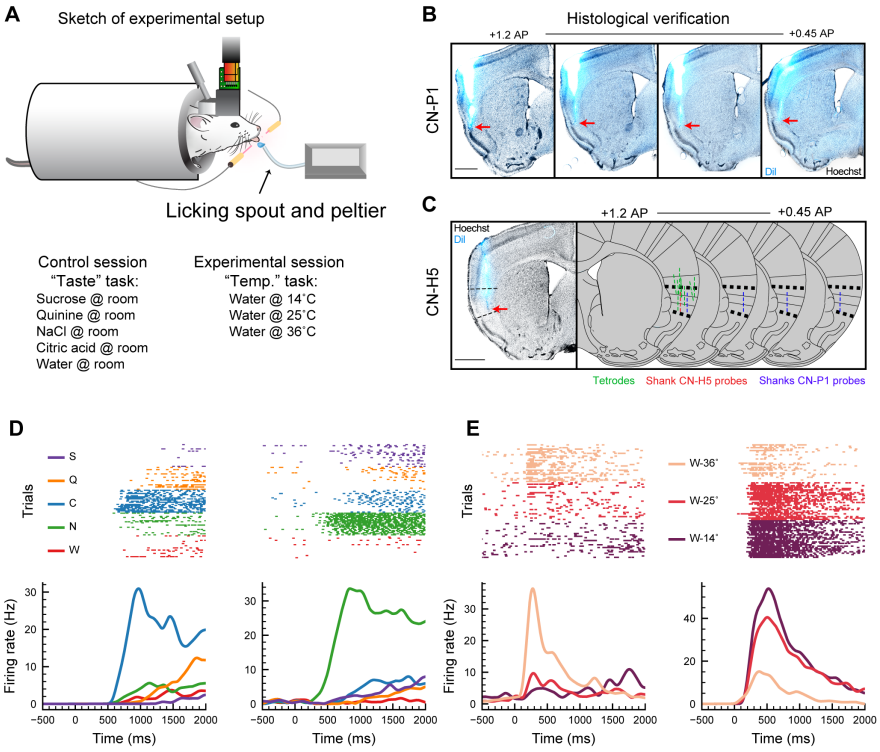

Figure 2: Quantification of water responses in the mouse GC. A: Sketch showing the recording setup and a head-restrained mouse licking a spout to obtain intraoral stimuli for two different conditions: the "control" and "experimental" session (see Materials and Methods). B: Example of histological sections showing the tracks (cyan) of the four shanks of the CN-P1 probe in the GC. Cyan arrows point to the tip of the probe. Scale bar is 1 mm. C: On the left, there is an example of one histological section showing a CN-H5 probe track (cyan) in the GC. Red arrow points to the tip of the probe. On the right there is a schematic of the summary of the tetrode and probes tracks from the 16 mice. Scale bar is 1 mm. D: Raster plots and PSTHs of 2 representative GC neurons recorded during the "control" session showing taste responses. Trials pertaining to different tastants are grouped together (in the raster plots) and color-coded (both in the raster plots and PSTHs), with sucrose (S) in purple, quinine (Q) in yellow, NaCl (N) in green, citric acid (C) in blue, and water (W) in red. E: Raster plots and peristimulus time histograms (PSTHs) of 2 representative GC neurons recorded during the "experimental" session showing thermal responses. Trials pertaining to water at different temperatures are grouped together (in the raster plots) and color-coded (both in the raster plots and PSTHs), with 14 °(W-14 °) in purple, 25 °(W-25 °) in red and 36 °(W-36 °C) in salmon.

neurons showed a fast onset, with firing rate significantly changing from baseline within the first 300 ms after stimulus delivery (Fig. 3E; mean onset 0.29 ± 0.360 s) and reaching the peak on average at 0.94 ± 0.65 s (Fig. 3E). Analysis of the distribution of two waveform properties (firing rate and trough to peak) revealed no differences in the population of neurons sampled via tetrodes and silicon probes (Fig. 3F; firing rate comparison - two-sample Kolmogorov-Smirnov test: D = 0.075617, p-value = 0.8809; trough to peak comparison - two-sample Kolmogorov-Smirnov test: D = 0.12461, p-value = 0.3065).

To investigate the relationship between neural activity and oral thermosensation, we evaluated whether single neuron GC responses depend upon the temperature of the stimulus. A qualitative evaluation of the raster plots and PSTHs in Figures 2 and 4 indicated that these responses can be temperature-independent (i.e., water responses appear to be similar at the three temperatures tested; see for example Fig. 4A) and temperature-dependent (i.e., evoked responses appear to encode temperature of water; see for example Fig. 4B and Fig. 2E). To quantify the degree of temperature specificity of GC water responses, we subjected each of the water-responsive neurons to a support vector machine (SVM) classifier (Neese et al., 2022; see Materials and Methods for more details). The SVM used a supervised machine learning algorithm that act as a classifier whose performance is a surrogate for the ability of each individual neuron to encode thermal information in a 1.5-s post-stimulus temporal window.

This analysis revealed that more than half of the GC water-responsive neurons (53.1%, 137/258) are temperature-dependent (Fig. 4C) whereas the remaining (46.9%, 121/258) likely encoded for thermal-independent somatosensory features. Next, we aimed to understand if the temperature-dependent GC neurons preferentially encoded only a single temperature or if they were capable of encoding information pertaining to multiple thermal stimuli. This analysis serves only to estimate how many GC neurons were modulated by more than one thermal stimulus, independent of the degree of the temperature. The distribution plot in Figure 4C indicates that the majority of water-dependent neurons are capable of encoding up to two thermal stimuli and rarely all three of the temperatures tested (Fig. 4C, right; Chi-squared test for given probabilities: X-squared = 43.635, df = 2, p-value = 3.348e-10; Multiple proportion comparison - Marascuilo procedure, p<0.05). Next, we wanted to evaluate if GC temperature-dependent neurons are tuned to both cooling and warming intraoral stimuli or if they preferentially respond to either one. When we considered the absolute values of the water stimulus (14 °, 25 °, or 36 °C), we observed that temperature-dependent neurons were broadly responsive to all thermal stimuli, independent of the degree (°C) value (Fig. 4C, left; Chi-squared test for given probabilities: X-squared = 0.010638, df = 2, p-value = 0.9947). If instead we consider deviation from resting oral temperature (32 °C (Leijon et al., 2019); ΔT), more GC neurons appear to be tuned to cooling (<32 °C) than to warming (>32

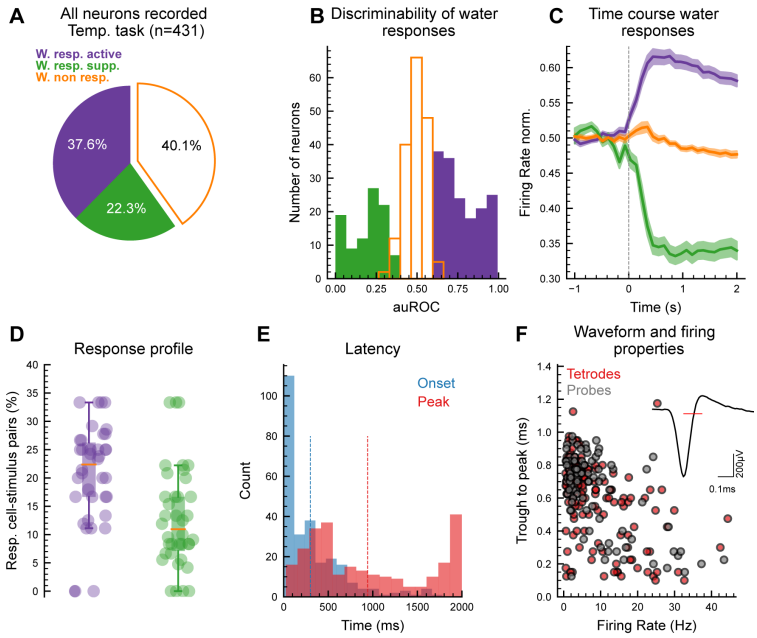

Figure 3: Quantification of water responses in the mouse GC. A: Pie chart displaying the proportion and distribution of single neurons showing either an excitatory (*W.resp. active* in purple) or inhibitory (*W.resp. supp.* in green) response to water. It is important to note that this analysis was performed on data averaged across temperatures, and therefore only serves to estimate whether and how GC was responsive to oral stimuli—not whether that response depended on the thermal properties of the stimulus. B: Histograms of the discriminability of water responses in the GC as assessed by response auROC (in which an auROC of 1 indicates excitatory response, and 0 indicates inhibitory response). Filled bars indicate significant responses. C: Population peristimulus time histograms (PSTHs) of excitatory (purple), inhibitory (green), and nonresponsive (orange) neurons expressed as normalized firing rate (norm. FR). Shaded areas represent SE. D: Percent of GC cell-stimulus pairs with significant activation or suppression across experimental sessions (exp. session n = 37). The box represents the lower and upper quartiles, the orange horizontal lines represent the median. Filled circles represent each data point. (Student Two Sample t-test; t = 3.7713, df = 74, p-value = 0.0003246). E: Distribution of water-evoked response onset (blue) and peak (red). Vertical dashed lines represent mean values. F: Scatter plot of the trough to peak duration and firing rate of all single neurons recorded. Red and gray dots represent neurons isolated from tetrode and probe recording sessions, respectively. The inset shows a representative example of a spike waveform with a red horizontal line highlighting the duration of the trough-to-peak interval.

°C) stimuli. However, this latter observation might be biased due to the limited and uneven (14 °C and 25 °C are "cooling" and 36 °C is "warming") set of stimuli used (see the Discussion section for more on this point).

To further investigate how GC temperature-dependent neurons were tuned to absolute changes in orally-sourced temperature of fluid solution, we performed an additional analysis: we evaluated if the neuron's firing either positively or negatively correlated with increase of temperature (monotonic) or not (non-monotonic). Our analysis revealed that the majority of water-responsive neurons change their firing rate in a monotonic fashion (Fig. 4D; Chi-squared test for given probabilities: X-squared = 10.782, df = 1, p-value = 0.001025).

These analyses revealed that most of the GC neurons that respond to the delivery of water are temperature-dependent and are capable of encoding different absolute temperature values in a mostly monotonic manner. These results are consistent with neurons in the GC processing thermosensory information from the oral cavity in absence of chemosensory stimuli.

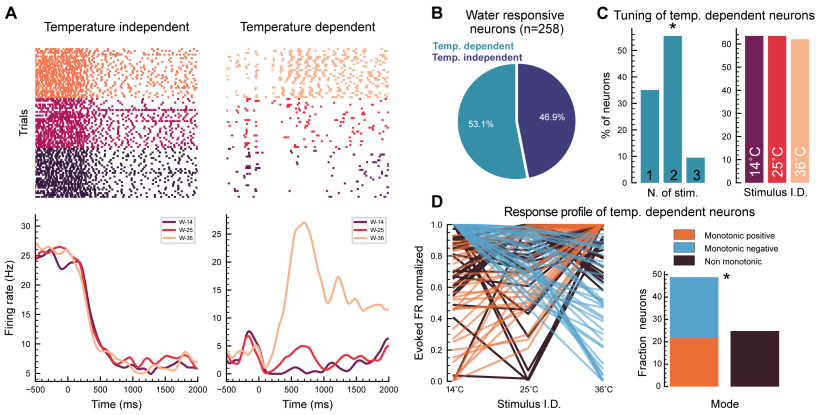

Figure 4: Tuning of temperature-selective neurons in the gustatory cortex (GC). A: Raster plots and peristimulus time histograms (PSTHs) of two representative water-responsive GC neurons, showing temperature-independent (left) and -dependent (right) responses. Trials pertaining to water at different temperatures are grouped together (in the raster plots) and color-coded (both in the raster plots and PSTHs), with 14 °(W-14 °) in purple, 25 °(W-25 °) in red and 36 °(W-36 °C) in salmon. B: Pie chart displaying the proportion of water-responsive neurons showing either temperature-dependent (in light blue) or -independent (in dark blue) response to water. C: *Left* - Fraction of temperature-dependent neurons responding to 1, 2, or 3, thermal stimuli (Chi-squared test for given probabilities: X-squared = 43.635, df = 2, p-value = 3.348e-10; Marascuilo procedure for pairs comparison: 1 vs 2, p value < 0.05 - 1 vs 3 and 2 vs 3, p-value < 0.05). *Right* - fraction of temperature-dependent neurons responding to the three different temperatures of water (Chi-squared test for given probabilities: X-squared = 0.010638, df = 2, p-value = 0.9947). D: *Left* - Plot of peak evoked firing rate (normalized) as a function of water temperature for all the water-dependent neurons. *Right* - Quantification of the mode (monotonic vs. non monotonic) of response for temperature-dependent neurons in the GC (Chi-squared test for given probabilities: X-squared = 10.782, df = 1, p-value = 0.001025)

Population coding for intraoral temperature in GC

To further characterize cortical thermosensory processing, we performed a population decoding analysis.

The decoder was instantiated using the same SVM classifier described above for single neurons; the difference in this case is that the classifier was trained using single trial responses of pseudopopulations (neurons pooled from different experimental sessions and animals) of temperature-dependent GC neurons and tested using a held-out method (training set consisting of 67% of the spike trains and a testing set consisting of the remaining 33% of the spike trains). This process was repeated 20 times (each time using different training and testing splits) to compute the decoding accuracy, defined as the fraction of trials in which the classifier made correct temperature predictions. We began by analyzing how well the population activity of temperature-dependent neurons (n = 135) represented

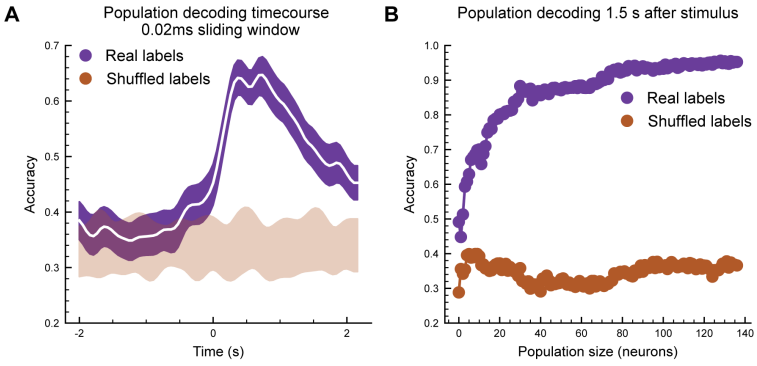

Figure 5: Tuning of temperature-selective neurons in the gustatory cortex (GC). A: Time course of decoding performance (white line) considering the population of temperature-dependent neurons. Purple shaded area indicates the 1%ile-99%ile range of the 20 times the decoder was ran, each time using different training and testing splits (n = 20). Brown shaded areas indicate the 1%ile-99%ile range of the decoding performance over time after shuffling (10 times) stimulus labels for all trials. B: Mean accuracy of SVM linear decoders trained to discriminate the three different temperatures (using a temporal window of 1.5 s after stimulus) as the decoder gained access to progressively more neurons (purple dots). Brown dots indicate the decoding performance over time after shuffling (10 times) stimulus labels for all trials

the three thermal stimuli over a 2-s long post-stimulus temporal window (Fig. 5A). Figure 5A shows the decoding performance of the pseudo-population using a sliding window of 50 ms (white trace [average accuracy over the 20 training and testing splits] over the purple shading [1%ile (lower bound) and 99%ile (upper bound) of the 20 training and testing splits]). As a control, the same analysis was performed other 1000 times after shuffling the thermal stimuli labels; the brown shaded area in Figure 5A show the 1%ile (lower bound) and 99%ile (upper bound) of the distribution of the control decoding values over time. The decoding time-course showed an early onset (classification above control) and reached its peak within 500 ms after stimulus delivery. In addition, although the overall classification value started decreasing after 500 ms, decoding performances remained above control until the end of the temporal window analyzed (Fig. 5A). Figure 5B shows how classification during a 1.5-s post-stimulus temporal window changed as the decoder gained access to progressively more neurons. While classifier trained with a small numbers of neurons were less accurate at identifying intraoral thermal information, increasing the number of neurons in the pseudo-population drastically increased the decoding performance, reaching up to 85% accuracy with less than 40 neurons (Fig. 5B, purple dots). As expected, the decoding performance obtained with the control data did not improve and stayed around chance level even when the decoder gained access to progressively more neurons (Fig. 5B, brown dots).

Taken together, these results indicate that both single and ensembles of temperature-dependent GC neurons rapidly and reliably encoded intraoral thermosensory signals over time, with classification accuracy for stimulus identity remaining above chance and control level for up to 2 s after stimulus delivery.

Spatial organization of intraoral thermal responses

Next, we sought to determine whether intraoral responses were topographically organized. A previous study in anesthetized rats suggested that thermal responses in the GC are mostly clustered in the dorsal (granular) region (Kosar et al., 1986). However, it is still unknown whether intraoral thermal responses in behaving mice are also organized with a seemingly topographical gradient along the dorso-ventral axes of the GC.

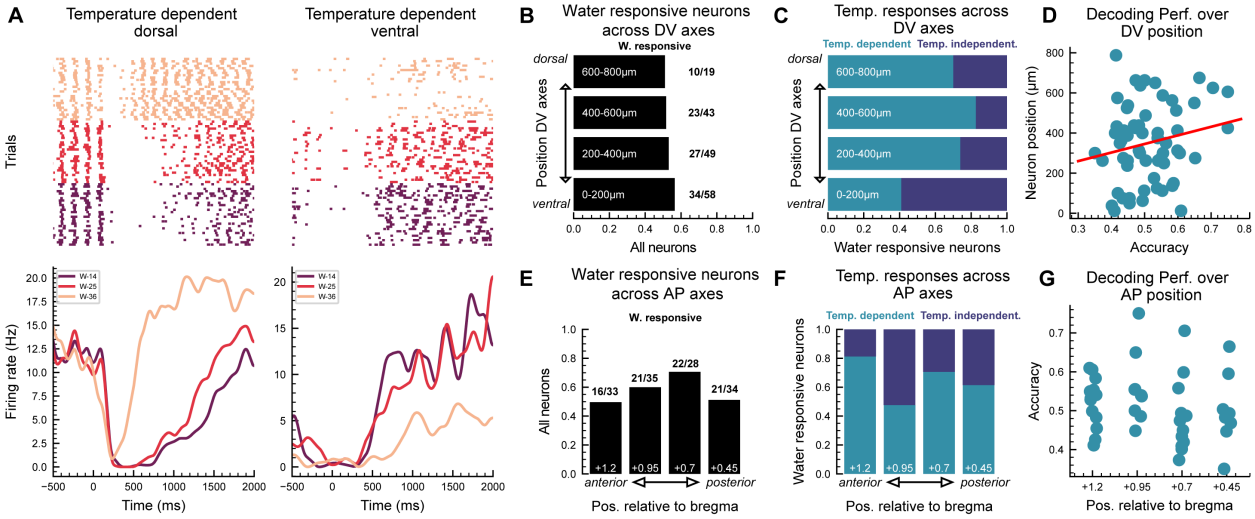

Figure 6: Tuning of temperature-selective neurons in the GC. A: Raster plots and PSTHs of two temperature-dependent neurons, one recorded in the dorsal (left) and one in the ventral (right) GC. Water delivery trials at different temperatures are grouped together (in the raster plots) and color-coded (both in the raster plots and PSTHs), with 14 °(W-14 °) in purple, 25 °(W-25 °) in red and 36 °(W-36 °C) in salmon. B: Fraction of water-responsive neurons recorded in four 200 µm bins along the GC dorso-ventral axes. C: Fraction of temperature-dependent and -independent neurons as a function of their dorso-ventral location (Chi-squared test for given probabilities: X-squared = 7.0667, df = 3, p-value = 0.0698). D: Scatter plot of the SVM accuracy for temperature-dependent neurons against their dorso-ventral location. E: Fraction of water-responsive neurons recorded in four 200 µm bins along the GC antero-posterior axes. F: Fraction of temperature-dependent and -independent neurons as a function of their antero-posterior location (Chi-squared test for given probabilities: X-squared = 1.3721, df = 3, p-value = 0.7121). G: Plot of the SVM accuracy for temperature-dependent neurons against their antero-posterior location.

To address this question, we took advantage of the recording sessions performed with chronic probes that allowed us to triangulate the location of the recorded neurons along to the dorso-ventral axes spanning up to 800 µm (see Materials and Methods section for more details). Visual inspection of spiking activity in

Figure 6A indicated the presence of temperature-dependent neurons in the dorsal and ventral region of the GC. We divided the dorso-ventral axes of the portion of the GC captured by our recording into four 200-µm spatial bins (Fig. 6B-C). Our post-hoc evaluation of the implant tracks confirmed that the most ventral position was well within the agranular region of the GC (Fig. 3B). Overall, our probes recording spanned 800 µm, which covered a large portion of the dorso-ventral plane of the mouse GC (Wang et al., 2020). AuROC analysis revealed that a similar fraction of recorded GC neurons within each spatial bin responded to water stimuli and were classified as "water-responsive" (Fig. 6B). Additional analysis of the temperature-dependent neurons along the GC dorso-ventral axes revealed they reflect a coarse topographical organization with much less temperature-dependent neurons in the most ventral part of GC (0-200 µm) compared to the other three spatial bins analyzed (Fig. 6C; 4-sample test for equality of proportions: X-squared = 12.463, df = 3, p-value = 0.005955). To further investigate between temperature-dependent neurons and their location along the GC dorso-ventral axes, we plotted the single neuron SVM decoding accuracy against the neuron position (Fig. 6D). We reasoned that a topographical clustering might also appear when considering the amount of thermal-related information (expressed as decoding accuracy) of the temperature-dependent neurons (for example, neurons with high accuracy could cluster more dorsally). Contrary to our prediction, visual inspection of Figure 6D and linear regression analysis ($R^2 = 0.0383$) revealed that was not the case. We then focused our attention on the organization of intraoral thermal responses along the rostro-caudal axes. Recent studies started to uncover the role of the mouse posterior Insular Cortex in skin warming and cooling (Vestergaard et al., 2022; Beukema et al., 2018). To determine if intraoral thermal responses in the GC are organized in a rostro-caudal gradient, we analyzed the temperature-dependent neurons recorded with the P1 probe (Fig. 2E) that allowed us to examine responsiveness along 1 mm of the GC antero-postero axes. Similar to what was shown above for the recording across the dorso-ventral axes, auROC analysis revealed that a similar fraction of recorded GC neurons within each spatial bin responded to water stimuli and were classified as "water-responsive" (Fig. 6E). Analysis of the distribution of temperature-dependent neurons (Fig. 6F) and their decoding performance along the antero-postero axes (Fig. 6G) revealed no apparent topographical organization (Fig. 6F ; 4-sample test for equality of proportions: X-squared = 3.5259, df = 3, p-value = 0.3174 - Fig. 6G ; one way ANOVA: F(3,30) = 1.135, p-value = 0.351).

In summary, these results suggest that the details of temperature-dependent responses and thermosensory coding are, for the most part, insensitive to anatomic location within the mouse GC. Our results revealed a coarse organization along the dorso-ventral axes and no apparent spatial distribution along the rostro-caudal one. Overall, these data demonstrate that, similar to other reports investigating distribution of taste responses (Levitan et al., 2019; Chen et al., 2021), intraoral thermosensory processing is distributed, rather than being clustered into distinct spatial sub-region.

Discussion

This study evaluated the neural representations of intraoral thermal stimuli in absence of taste in the GC of behaving mice. We observed that GC neurons were capable of reliably responding to and discriminating a wide range of innocuous intraoral temperatures in a mostly monotonic manner. With the exception of the most ventral region, thermal responses were spatially distributed across GC. Altogether, our findings demonstrate the GC of behaving mice is involved in processing intraoral information important to ingestive behaviors. This work represents the first effort to reveal details of the cortical code for the mammalian intraoral thermosensory system in behaving mice and paves the way for future investigations on the cortical circuits and operational principles underlying thermogustation.

Oral thermosensory coding in GC

Our results indicate that the GC integrates a massive amount of thermal information in the absence of a taste stimulus. More than half of the GC neurons that are modulated by the contact of a 4 µl droplet of water within the oral cavity are temperature-dependent (Fig. 4B). If we considered the temperatures used in our study in absolute terms, we observed GC responses to all three temperatures with often the same neurons capable of representing more than one stimulus (Fig. 4C). When considering the degree of thermal change (i.e., ΔT) achieved during stimulation from resting oral temperature [32 °C, (Leijon et al., 2019)], more GC neurons appear to be tuned to cooling (<32 °C) than to warming (>32 °C) stimuli. One challenge

in the interpretation of this latter point is that we have not tested if our results generalize across a wider range of temperatures. For example, recent *in vivo* studies have shown that a subset of neurons in the trigeminal ganglion and the parabrachial nucleus of the pons (PBN) also respond to noxious cold (<14 °C) and hot (>40 °C) intraoral stimuli (Yarmolinsky et al., 2016; Lemon et al., 2016; Leijon et al., 2019; Li and Lemon, 2019; Lemon, 2021). The experimental design of the current work did not allow this level of analysis. We purposefully chose to omit noxious thermal stimuli to avoid distress for the mice and allow them to be engaged in the task and actively lick for a substantial number of trials. Another possibility is that GC mostly encodes the hedonic properties of intraoral temperature. Along this line, it is well established that GC neurons are capable of representing palatability of intraoral taste stimuli (Katz et al., 2001) and that cooler temperatures of fluid solutions are preferred by water deprived rodents (Torregrossa et al., 2012).

Spatial organization of orally-sourced thermal responses

Pioneering works in anesthetized rats have indicated that changes in intraoral temperature modulate the activity of a subset of GC neurons (Kosar et al., 1986; Yamamoto et al., 1981). Interestingly, Kosar et al. provided some experimental evidence in support of a clear topographical organization of responses to intraoral stimuli. Their findings showed that, in the GC of anesthetized rats, thermal responses were not organized in a rostro-caudal fashion but appeared to be clustered dorsally (granular portion of the GC) with taste responses exclusively clustered in the ventral agranular region. To evaluate if intraoral thermal responses are topographically organized in the mouse GC, we performed a subset of electrophysiological recordings using linear and multi-shank silicon probes. With this approach we relied on the high density of electrode contacts that allowed us to detect each spike at multiple sites, providing an opportunity to "triangulate" the location of each spike and to infer the relative 3D position of each single neuron. Our data revealed temperature-dependent activity is distributed with the exception of the most ventral portion of the GC where there were more neurons responding to water in a temperature-independent manner (Fig. 6C). In addition, single neuron decoding revealed that the amount of temperature-dependent information did not depend on the dorso-ventral position of the neuron (Fig. 6D). These findings appear to be partially in conflict with the one from Kosar et al. for at least two reasons. First, as already mentioned above, the distribution of temperature-dependent neurons in our study appears for the most part uniform. Second, during our "control session" we observed response to taste in the most dorsal and ventral part of GC. This latter result - while in conflict with Kosar et al. where taste responses appeared to be clustered ventrally - is in agreement with other studies in mice showing that spatial location plays no role in the distribution of taste responses (Levitan et al., 2019; Chen et al., 2021). It is important to highlight that the apparent lack of topographical organization of thermosensory responses does not exclude the possibility of the existence of subtle differences between GC subregions or between the GC of different rodents. Future experiments would help to further elucidate whether responses to both cues are generally non-overlapping and occupy successively more ventral positions in the cortex, and if there is a functional difference between the GC in mice and rats.

Origin of thermosensory responses in the GC

It is likely that one of the neural circuits allowing thermal information to reach the GC is in part the ascending gustatory pathway. Intraoral temperature stimulation can stimulate somatosensory neurons of the trigeminal system, which are responsible for thermosensation of all oral surfaces (Lemon, 2021). *In vivo* experiments in mice have revealed that neurons in the trigeminal ganglia are highly sensitive to innocuous and noxious cooling (Yarmolinsky et al., 2016; Leijon et al., 2019; Lemon et al., 2016). Interestingly, while a subset of trigeminal ganglia neurons are also sensitive to noxious heat, comparably fewer cells respond to innocuous warming (Yarmolinsky et al., 2016; Leijon et al., 2019). In rodents, neurons in the trigeminal ganglia activate second-order trigeminal neurons that project to the PBN - a brain region that is also part of the ascending gustatory pathway (PBN receives taste inputs from the nucleus of the solitary tract). A recent study has discovered that some trigeminal inputs supplying craniofacial somatosensation reach the same PBN neurons receiving gustatory inputs (Li and Lemon, 2019). It is important to note that these trigeminal inputs reached PBN neurons that display sensitivity to aversive oral temperatures and tastes, highlighting the putative role of the PBN in processing and relaying supported a multimodal intraoral sensory information including gustatory, nociceptive, and thermal stimuli (Li et al., 2022). Thermal stimulation inside the

mouth can also recruit taste-sensitive nerves. On the one hand, temperature can influence the peripheral taste-sensitive neurons in presence of gustatory stimuli via the warmth-activated transient receptor potential (TRP) melastatin 5 (TRPM5) cation channel (involved with GPCR-mediated transduction cascades for sweet, umami, and bitter taste stimuli) (Talavera et al., 2005; Zhang et al., 2003) and the thermal-sensitive epithelial sodium channels (ENaCs) (involved with sodium taste transduction) (Askwith et al., 2001). On the other hand, temperature can influence the peripheral taste-sensitive neurons even in absence of taste - a condition that is more relevant to the data presented in our study. Experimental evidence indicated that a subset of chorda tympani neurons that do not respond to gustatory stimuli can be activated by cold fluid applied to the tip of the tongue (Yokota and Bradley, 2016, 2017). In addition, electrophysiological recordings of chorda tympani nerves in taste-deficient mice revealed oral thermal responses (Finger et al., 2005). Future studies combining cell-type, molecular and circuit manipulation approaches will be key to unravel more details of the intraoral thermal pathway.

A taste of things to come

In the past three decades, multiple studies have shed important light on the taste responses of GC neurons in awake rodents (Samuelsen and Vincis, 2021). Extracellular recordings and two-photon experiments have extensively and convincingly described both the temporal and spatial profile of taste-evoked activity. For example, electrophysiological data highlighted the importance of hundreds of milliseconds- and seconds-long temporal dynamics of taste-evoked spiking activity (Katz et al., 2001; Gutierrez et al., 2010; Neese et al., 2022), while imaging experiments revealed the lack of chemotopic topographical organization of these responses (Chen et al., 2021). However, these results originated from studies in which taste stimuli are experienced at a single temperature. While this approach has shaped our understanding of cortical taste processing, it provides only a partial picture of the functional features of the GC. It is a common experience that temperature is a cue relevant to food preference and multiple studies have shown temperature's influence on taste perception (Moskowitz, 1973; Bartoshuk et al., 1982; Green and Frankmann, 1987; Torregrossa et al., 2012). In addition, our results indicated that GC activity is strongly modulated by intraoral fluid temperature. For all of these reasons, it is reasonable to wonder whether GC taste tuning, as well as the temporal and spatial properties of taste responses, are altered by the temperature of the stimulus and to what extent. Future experiments will examine the GC functional organization of chemosensory gustatory responses with respect to temperature-taste integration.

Acknowledgments

This work was supported by funding from the National Institute of Deafness and Other Communication Disorders of the National Institute of Health Grant R01DC019326 to R.V. and Grant T32 DC000044 to C.G.B. The authors would also like to acknowledge Dr. Chris Lemon, Dr. Richard Bertram and the members of the Vincis laboratory for their feedback and insightful comments. Portion of these data were presented in abstract form at the 2021 meeting of the Association for Chemoreception Sciences, Bonita Spring, FL.

Author contribution: C.G.B and R.V. designed research; C.G.B performed research; C.G.B, C.N. and R.V. analyzed data; R.V. wrote the first draft of the paper; C.G.B., C.N. and R.V. edited the paper; R.V. wrote the paper.

The authors declare no competing financial interest.

Correspondence should be addressed to: rvincis@fsu.edu

References

Allchorne AJ, Broom DC, Woolf CJ (2005) Detection of cold pain, cold allodynia and cold hyperalgesia in freely behaving rats. *Molecular pain* 1:1744–8069.

Arieli E, Gerbi R, Shein-Idelson M, Moran A (2020) Temporally-precise basolateral amygdala activation is required for the formation of taste memories in gustatory cortex. *The Journal of Physiology* 598:5505–5522.

Askwith CC, Benson CJ, Welsh MJ, Snyder PM (2001) Deg/enac ion channels involved in sensory transduction are modulated by cold temperature. *Proceedings of the National Academy of Sciences* 98:6459–6463.

Bartoshuk L, Rennert K, Rodin J, Stevens J (1982) Effects of temperature on the perceived sweetness of sucrose. *Physiology & Behavior* 28:905–910.

Beukema P, Cecil KL, Peterson E, Mann VR, Matsushita M, Takashima Y, Navlakha S, Barth AL (2018) Trpm8-mediated somatosensation in mouse neocortex. *Journal of Comparative Neurology* 526:1444–1456.

Bouaichi CG, Vincis R (2020) Cortical processing of chemosensory and hedonic features of taste in active licking mice. *Journal of neurophysiology* 123:1995–2009.

Buccino AP, Hurwitz CL, Garcia S, Magland J, Siegle JH, Hurwitz R, Hennig MH (2020) Spikeinterface, a unified framework for spike sorting. *Elife* 9:e61834.

Cerf-Ducastel B, Van de Moortele PF, MacLeod P, Le Bihan D, Faurion A (2001) Interaction of gustatory and lingual somatosensory perceptions at the cortical level in the human: a functional magnetic resonance imaging study. *Chemical Senses* 26:371–383.

Chen K, Kogan JF, Fontanini A (2021) Spatially distributed representation of taste quality in the gustatory insular cortex of behaving mice. *Current Biology* 31:247–256.

De Araujo IE, Kringelbach ML, Rolls ET, McGlone F (2003) Human cortical responses to water in the mouth, and the effects of thirst. *Journal of neurophysiology* 90:1865–1876.

Dotson CD, Colbert CL, Garcea M, Smith JC, Spector AC (2012) The consequences of gustatory deafferentation on body mass and feeding patterns in the rat. *American Journal of Physiology-Regulatory, Integrative and Comparative Physiology* 303:R611–R623.

Finger TE, Danilova V, Barrows J, Bartel DL, Vigers AJ, Stone L, Hellekant G, Kinnamon SC (2005) Atp signaling is crucial for communication from taste buds to gustatory nerves. *Science* 310:1495–1499.

Green BG, Frankmann SP (1987) The effect of cooling the tongue on the perceived intensity of taste. *Chemical Senses* 12:609–619.

Guest S, Grabenhorst F, Essick G, Chen Y, Young M, McGlone F, de Araujo I, Rolls ET (2007) Human cortical representation of oral temperature. *Physiology & behavior* 92:975–984.

Gutierrez R, Simon SA, Nicolelis MA (2010) Licking-induced synchrony in the taste–reward circuit improves cue discrimination during learning. *Journal of Neuroscience* 30:287–303.

Jezzini A, Mazzucato L, La Camera G, Fontanini A (2013) Processing of hedonic and chemosensory features of taste in medial prefrontal and insular networks. *Journal of Neuroscience* 33:18966–18978.

Katz DB, Simon S, Nicolelis MA (2001) Dynamic and multimodal responses of gustatory cortical neurons in awake rats. *Journal of Neuroscience* 21:4478–4489.

Kay KE, Martin LE, James KF, Haygood SM, Torregrossa AM (2020) Temperature is sufficient to condition a flavor preference for a cold-paired solution in rats. *Chemical Senses* 45:563–572.

Kemp SE, Beauchamp GK (1994) Flavor modification by sodium chloride and monosodium glutamate. *Journal of Food Science* 59:682–686.

Kosar E, Grill HJ, Norgren R (1986) Gustatory cortex in the rat. i. physiological properties and cytoarchitecture. *Brain research* 379:329–341.

Leijon SC, Neves AF, Breza JM, Simon SA, Chaudhari N, Roper SD (2019) Oral thermosensing by murine trigeminal neurons: modulation by capsaicin, menthol and mustard oil. *The Journal of physiology* 597:2045–2061.

Lemon CH (2021) Tasting temperature: neural and behavioral responses to thermal stimulation of oral mucosa. *Current opinion in physiology* 20:16–22.

Lemon CH, Kang Y, Li J (2016) Separate functions for responses to oral temperature in thermo-gustatory and trigeminal neurons. *Chemical senses* 41:457–471.

Levitan D, Lin JY, Wachutka J, Mukherjee N, Nelson SB, Katz DB (2019) Single and population coding of taste in the gustatory cortex of awake mice. *Journal of neurophysiology* 122:1342–1356.

Li J, Ali MSS, Lemon CH (2022) Trpv1-lineage somatosensory fibers communicate with taste neurons in the mouse parabrachial nucleus. *Journal of Neuroscience* 42:1719–1737.

Li J, Lemon CH (2019) Mouse parabrachial neurons signal a relationship between bitter taste and nociceptive stimuli. *Journal of Neuroscience* 39:1631–1648.

Liu H, Fontanini A (2015) State dependency of chemosensory coding in the gustatory thalamus (vpmpc) of alert rats. *Journal of Neuroscience* 35:15479–15491.

Lopes G, Bonacchi N, Frazão J, Neto JP, Atallah BV, Soares S, Moreira L, Matias S, Itskov PM, Correia PA et al. (2015) Bonsai: an event-based framework for processing and controlling data streams. *Frontiers in neuroinformatics* 9:7.

Maier JX (2017) Single-neuron responses to intraoral delivery of odor solutions in primary olfactory and gustatory cortex. *Journal of Neurophysiology* 117:1293–1304.

Moskowitz HR (1973) Effects of solution temperature on taste intensity in humans. *Physiology & Behavior* 10:289–292.

Mukherjee N, Wachutka J, Katz DB (2019) Impact of precisely-timed inhibition of gustatory cortex on taste behavior depends on single-trial ensemble dynamics. *Elife* 8:e45968.

Neese C, Bouaichi CG, Needham T, Bauer M, Bertram R, Vincis R (2022) Active licking shapes cortical taste coding. *Journal of Neuroscience* 42.

Pachitariu M, Steinmetz NA, Kadir SN, Carandini M, Harris KD (2016) Fast and accurate spike sorting of high-channel count probes with kilosort. *Advances in neural information processing systems* 29.

Roussin AT, D'Agostino AE, Fooden AM, Victor JD, Di Lorenzo PM (2012) Taste coding in the nucleus of the solitary tract of the awake, freely licking rat. *Journal of Neuroscience* 32:10494–10506.

Rudenga K, Green B, Nachtigal D, Small D (2010) Evidence for an integrated oral sensory module in the human anterior ventral insula. *Chemical senses* 35:693–703.

Samuelsen CL, Fontanini A (2017) Processing of intraoral olfactory and gustatory signals in the gustatory cortex of awake rats. *Journal of Neuroscience* 37:244–257.

Samuelsen CL, Gardner MP, Fontanini A (2013) Thalamic contribution to cortical processing of taste and expectation. *Journal of Neuroscience* 33:1815–1827.

Samuelsen CL, Vincis R (2021) Cortical hub for flavor sensation in rodents. *Frontiers in Systems Neuroscience* .

Schier LA, Spector AC (2019) The functional and neurobiological properties of bad taste. *Physiological reviews* 99:605–663.

Small DM (2012) Flavor is in the brain. *Physiology & behavior* 107:540–552.

Small DM, Voss J, Mak YE, Simmons KB, Parrish T, Gitelman D (2004) Experience-dependent neural integration of taste and smell in the human brain. *Journal of Neurophysiology* 92:1892–1903.

Spector AC, Travers SP (2005) The representation of taste quality in the mammalian nervous system. *Behavioral and cognitive neuroscience reviews* 4:143–191.

Stapleton JR, Lavine ML, Wolpert RL, Nicolelis MA, Simon SA (2006) Rapid taste responses in the gustatory cortex during licking. *Journal of Neuroscience* 26:4126–4138.

Suzuki R, Hunt SP, Dickenson AH (2003) The coding of noxious mechanical and thermal stimuli of deep dorsal horn neurones is attenuated in nk1 knockout mice. *Neuropharmacology* 45:1093–1100.

Talavera K, Yasumatsu K, Voets T, Droogmans G, Shigemura N, Ninomiya Y, Margolskee RF, Nilius B (2005) Heat activation of trpm5 underlies thermal sensitivity of sweet taste. *Nature* 438:1022–1025.

Torregrossa AM, Bales MB, Breza JM, Houpt TA, Smith JC, Contreras RJ (2012) Water restriction and fluid temperature alter preference for water and sucrose solutions. *Chemical senses* 37:279–292.

Verhagen JV, Kadohisa M, Rolls ET (2004) Primate insular/opercular taste cortex: neuronal representations of the viscosity, fat texture, grittiness, temperature, and taste of foods. *Journal of neurophysiology* 92:1685–1699.

Vestergaard M, Carta M, Poulet J (2022) The cellular coding of temperature in the mammalian cortex. *bioRxiv* .

Vincis R, Chen K, Czarnecki L, Chen J, Fontanini A (2020) Dynamic representation of taste-related decisions in the gustatory insular cortex of mice. *Current Biology* 30:1834–1844.

Vincis R, Fontanini A (2016) A gustocentric perspective to understanding primary sensory cortices. *Current opinion in neurobiology* 40:118–124.

Vincis R, Fontanini A (2019) Central taste anatomy and physiology. *Handbook of clinical neurology* 164:187–204.

Wang L, Zhang Z, Chen J, Manyande A, Haddad R, Liu Q, Xu F (2020) Cell-type-specific whole-brain direct inputs to the anterior and posterior piriform cortex. *Frontiers in neural circuits* 14:4.

Yamamoto T, Yuyama N, Kawamura Y (1981) Cortical neurons responding to tactile, thermal and taste stimulations of the rat's tongue. *Brain research* 221:202–206.

Yarmolinsky DA, Peng Y, Pogorzala LA, Rutlin M, Hoon MA, Zuker CS (2016) Coding and plasticity in the mammalian thermosensory system. *Neuron* 92:1079–1092.

Yokota Y, Bradley RM (2016) Receptive field size, chemical and thermal responses, and fiber conduction velocity of rat chorda tympani geniculate ganglion neurons. *Journal of Neurophysiology* 115:3062–3072.

Yokota Y, Bradley RM (2017) Geniculate ganglion neurons are multimodal and variable in receptive field characteristics. *Neuroscience* 367:147–158.

Zhang Y, Hoon MA, Chandrashekar J, Mueller KL, Cook B, Wu D, Zuker CS, Ryba NJ (2003) Coding of sweet, bitter, and umami tastes: different receptor cells sharing similar signaling pathways. *Cell* 112:293–301.